A Cost-Effective Sideslip Estimation Method Using Velocity Measurements from Two GPS Receivers

Jong-Hwa Yoon and Huei Peng

***Abstract*— This paper demonstrates that the vehicle sideslip can be estimated through the kinematic relationship of velocity measurements from two low-cost GPS (Global Positioning System) receivers. To compensate for the low update rate of low-cost GPS receivers, acceleration/angular rate measurements from an IMU (Inertial Measurement Unit) are merged with the GPS measurements using an Extended Kalman Filter. Two technical challenges were addressed: (i) unsynchronized updates of the two GPS receivers and (ii) significant delays in GPS velocity measurement. A stochastic observability analysis reveals that the proposed method guarantees the observability when a vehicle has non-zero yaw rates. Experimental verification shows that the vehicle sideslip is estimated regardless of surface friction levels under several maneuvers.**

***Index Terms*—Sideslip estimation, Global Positioning System (GPS), Kalman Filter, Stochastic Observability**

I. INTRODUCTION

Electronic Stability Control (ESC) is a highly effective active safety system for ground vehicles. A study from the National Highway Traffic Safety Administration (NHTSA) reports that ESC can save 5,300~9,600 lives and prevent 156,000~238,000 injuries annually in the United States [1]. The vehicle sideslip angle is the angle between the vehicle's moving direction (course angle) and its heading direction (heading angle) at the center of mass. It is a critical piece of information for ESC implementation [2], yet is difficult/expensive to measure directly. Many approaches have been proposed toward its estimation and they can be grouped into three categories: Dynamic model-based, IMU integration-based, and GPS-based.

Dynamic model-based methods utilize a vehicle dynamic model that describes how the sideslip angle is affected by and related to vehicle input signals and parameters, such as steering angle and tire cornering stiffness. Farrelly proposed a standard Luenberger observer of a linearized system [3]. Kiencke showed the feasibility of a nonlinear observer [4]. Best showed that simultaneous estimation of cornering stiffness enhanced sideslip angle estimation performance [5]. Stephan compared the estimation performance of four types of observers (linear, extended Luenberger, extended Kalman filter, and sliding-mode) and concluded that nonlinear observers outperformed linear observers [6]. Yih proposed to use steering torque information for a sideslip angle estimation [7]. Gao showed that a high-gain observer based on input-output linearization was useful [8]. Grip proposed a nonlinear observer with a friction adaptation [9]. The dynamic model-based methods have two drawbacks: they require accurate vehicle parameter information such as tire cornering stiffness and vehicle mass, and they work only when the sideslip angle is small (roughly 4 degrees or less) [10].

IMU integration-based methods process signals of the Inertial Measurement Unit (IMU) to estimate the vehicle sideslip angle. Farrelly was among the first groups using this method [3]. He showed that sideslip angle estimation was robust to cornering stiffness variations. It was also shown that this method worked for large sideslip angles. Imsland proposed a nonlinear observer [11]. Ungoren confirmed the robustness of IMU integration-based methods for various sideslip angle ranges [12]. This type of method does not require accurate parameters and works well even for large sideslip angles. However, bias in the sensor measurement can significantly deteriorate the estimation accuracy because IMU integration-based methods rely heavily on measurement integration.

Several researchers have used GPS measurements for sideslip angle calculation. Since GPS technology can measure vehicle velocity via the Doppler effect, the course angle is directly measurable. Therefore, the main problem for GPS-based methods is to measure or estimate the vehicle heading angle. Bevly developed a method of utilizing a single-antenna GPS receiver for sideslip angle estimation [13-15]. His method merged the velocity signal from a low-cost single-antenna GPS receiver with accelerations and angular rates from an IMU. In his method, the vehicle heading is obtained by integrating the yaw rate during turning. Hrovat and Farrell focused on the accurate positioning capability of a GPS technology [16-17]. In their work, a vehicle was equipped with multiple GPS receivers. If the position of each GPS receiver is accurately known, the vehicle heading angle can be calculated from the relative positions among the receivers. Currently, the carrier-phase differential GPS (CDGPS) can meet the position accuracy requirement (position error within the range of centimeters) [17]. To achieve that accuracy, however, a base tower is required and the associated cost is

J.-H. Yoon is with TRW Automotive, 12000 Tech Center Dr., Livonia, MI 48150, USA (e-mail: jong.yoon@trw.com)

H. Peng is with the Department of Mechanical Engineering, G041 Lay Automotive Laboratory, University of Michigan, Ann Arbor, MI 48109 USA (e-mail: hpeng@umich.edu)

significant (at least several thousand dollars). Ryu utilized another aspect of CDGPS; measuring the heading angle from the observed phase difference of carrier waves received at two antennas. As the course and heading angles are measured by a dual antenna GPS receiver, the vehicle sideslip angle can be easily obtained [18-19]. This method solves most concerns of the previous methods but the dual-antennae CDGPS receiver is too expensive to be adopted by car makers today [20].

This paper proposes a new method to estimate the vehicle sideslip angle by using velocity measurements from two GPS receivers. GPS velocity measurements can be accurate regardless of GPS positioning accuracy because a GPS receiver determines velocity based on the Doppler shift of GPS carrier wave or by differencing two consecutive GPS carrier wave measurements, instead of differentiation of the GPS position measurements [13]. Since this method uses two GPS receivers, it may look similar to Ryu's method. However we only use the velocity measurement, which is accurate even on low-cost GPS receivers (Fig. 1). Benefits of this method include: (i) it does not require accurate vehicle parameter information, (ii) it works for large and small sideslip angles, (iii) it has GPS measurements correct the sideslip estimation during vehicle turning, (iv) it does not need a standing reference tower and (v) it is based on cost effective GPS receivers.

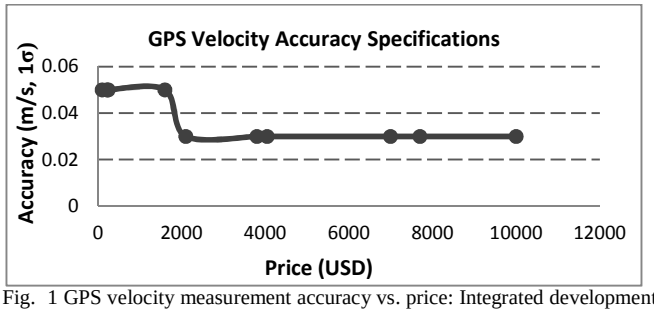

Fig. 1 GPS velocity measurement accuracy vs. price: Integrated development kits of San Jose Tech, NavSync, VBOX, Novatel, and Dewetron are compared.

The remainder of this paper is organized as follows. Section II describes how velocities of two GPS receivers are related to the vehicle sideslip angle. Section III shows the Kalman Filter implementation to integrate velocities of two GPS receivers and accelerations/angular rates of an IMU. Unsynchronized updates of two GPS receivers and significant delays in GPS measurements are addressed here. Section IV discusses the stochastic observability of the Kalman Filter. Section V presents results of experimental verification and discusses the performance in a statistical context. Conclusions are presented in Section VI.

II. VELOCITY MEASUREMENTS OF TWO RECEIVERS

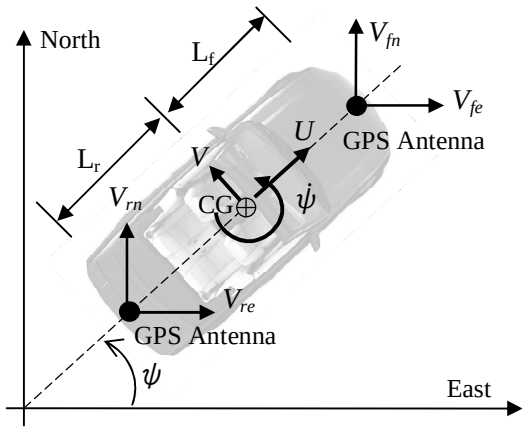

Fig. 2 Top view of a ground vehicle with two GPS receivers

Fig. 2 shows the top view of a ground vehicle with two GPS receivers installed at the front and rear ends of the vehicle. V_{fe}/V_{fn} and V_{re}/V_{rn} are eastbound/northbound velocities of the GPS receivers at the front and rear end, respectively. U and V are longitudinal and lateral velocities of the vehicle at center of gravity (CG). ψ is the vehicle yaw angle and $\dot{\psi}$ is the yaw rate. L_f and L_r are distances from CG to front and rear end GPS receivers, respectively. Velocities measured from the two GPS receivers are kinematically related to the vehicle longitudinal/lateral velocities, the yaw angle, and the yaw rate $(U,V,\psi,\dot{\psi})$ as

$$V_{fe} = U\cos\psi - (V + L_f\dot{\psi})\sin\psi \quad (1)$$

$$V_{fn} = U\sin\psi + (V + L_f\dot{\psi})\cos\psi \quad (2)$$

$$V_{re} = U\cos\psi - (V - L_r\dot{\psi})\sin\psi \quad (3)$$

$$V_{rn} = U\sin\psi + (V - L_r\dot{\psi})\cos\psi \quad (4)$$

U and V can be expressed as functions of $(V_{fe},V_{fn},V_{re},V_{rn})$ and the vehicle sideslip is

$$\beta = \tan^{-1}\left(V/U\right) \quad (5)$$

However, this equation set is not always solvable due to the singular point. To find the singular point(s), the Multivariable Taylor's Theorem [21] is applied to yield (6) where δ is deviation from the true value. The Jacobian matrix (the 4-by-4 matrix in (6)) expresses the relationship between infinitesimal change of $(U,V,\psi,\dot{\psi})$ and $(V_{fe},V_{fn},V_{re},V_{rn})$.

$$\begin{bmatrix}\delta V_{fe}\\ \delta V_{fn}\\ \delta V_{re}\\ \delta V_{rn}\end{bmatrix} = \begin{bmatrix}\cos\psi & -\sin\psi & -U\sin\psi - (V + L_f\dot{\psi})\cos\psi & -L_f\sin\psi\\ \sin\psi & \cos\psi & U\cos\psi - (V + L_f\dot{\psi})\sin\psi & L_f\cos\psi\\ \cos\psi & -\sin\psi & -U\sin\psi - (V - L_r\dot{\psi})\cos\psi & L_r\sin\psi\\ \sin\psi & \cos\psi & U\cos\psi - (V - L_r\dot{\psi})\sin\psi & -L_r\cos\psi\end{bmatrix}\begin{bmatrix}\delta U\\ \delta V\\ \delta\psi\\ \delta\dot{\psi}\end{bmatrix} \quad (6)$$

If the Jacobian does not have full rank, change in $(U,V,\psi,\dot{\psi})$ may not be manifested by measuring $(V_{fe},V_{fn},V_{re},V_{rn})$. This is the singular condition. Since the determinant of the Jacobian has a simple form of (7), (6) is singular if and only if the vehicle yaw rate is zero.

$$\det(J)=\left(L_f+L_r\right)^2\dot{\psi} \tag{7}$$

Fig. 3 gives an intuitive explanation why a zero yaw rate corresponds to the singular condition. When the vehicle yaw rate is zero, velocities of the two GPS receivers will be identical for two distinct cases of A and B. Therefore, it is impossible to calculate the vehicle yaw angle when the yaw rate is zero. In other words, velocities of the two GPS receivers need to be coupled with the yaw angle through a non-zero yaw rate.

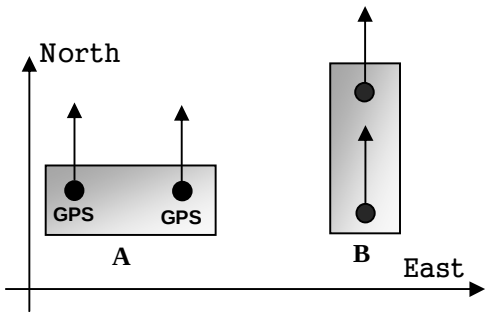

Fig. 3 Top view of two vehicles with different yaw angles when yaw rate is zero

When the vehicle yaw rate is not zero, $(\delta U,\delta V,\delta\psi,\delta\dot{\psi})$ are unique functions of $(\delta V_{fe},\delta V_{fn},\delta V_{re},\delta V_{rn})$ by inverting (6). Assuming that the standard deviations of $(\delta V_{fe},\delta V_{fn},\delta V_{re},\delta V_{rn})$ are identical, the standard deviation of the vehicle sideslip estimation is

$$\sigma_{GPS}^{-}\sqrt{\frac{L_f^2+L_r^2}{L_{sum}^2U^2}+\frac{2}{L_{sum}^2\dot{\psi}^2}}\le\sigma(\delta\beta)\le\sigma_{GPS}^{+}\sqrt{\frac{L_f^2+L_r^2}{L_{sum}^2U^2}+\frac{2}{L_{sum}^2\dot{\psi}^2}} \tag{8}$$

where

σ_{GPS}^{+}	$\sqrt{\sigma^2(\delta V_{GPS})+\lvert cov(\delta V_e,\delta V_n)\rvert}$
σ_{GPS}^{-}	$\sqrt{\sigma^2(\delta V_{GPS})-\lvert cov(\delta V_e,\delta V_n)\rvert}$
$\sigma(\delta V_{GPS})$	Standard deviation of the GPS velocity errors
$cov(\delta V_e,\delta V_n)$	Covariance of east-/north-bound GPS velocity errors
L_{sum}	$L_{f+}L_r$

Since the east-/north-bound velocities are measurements from the same GPS receiver, their errors are correlated and the covariance cannot be assumed to be zero. In the equation above, $\mathrm{cov}(\delta V_e,\delta V_n)$ of the front and rear end GPS receivers are assumed to be same (see the Appendix for the derivation). Equation (8) shows that the vehicle sideslip estimation using (1)-(5) becomes more accurate as the vehicle velocity and yaw rate increases.

III. SENSOR FUSION THROUGH KALMAN FILTER

Section II explains that longitudinal/lateral velocities (hence the vehicle sideslip angle) can be calculated by processing velocities from two GPS receivers as long as the vehicle is turning. In order to capture all of the vehicle dynamic modes, GPS update rate must be at least 10 Hz [13]. However, our market survey revealed that low cost GPS receivers are likely to have low update rates such as below 5Hz (Fig. 4). In fact, the GPS receivers utilized for this paper have a 2.5 Hz update rate.

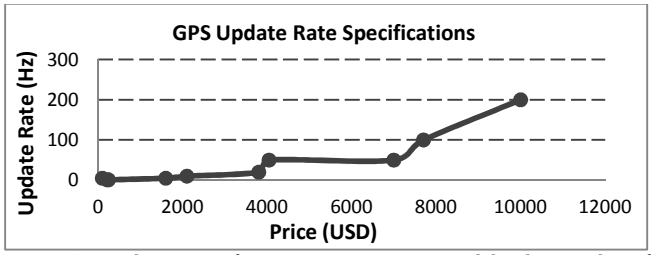

Fig. 4 GPS update rate performance vs. price: Integrated development kits of San Jose Tech, NavSync, VBOX, Novatel, and Dewetron are compared.

To compensate for the slow update rate, GPS measurements are merged with fast updating angular rates/accelerations from an IMU. As explained in [13], GPS velocities and IMU signals are an ideal pair for sensor fusion due to their complementary nature. The Kalman Filter is used as the sensor fusion framework.

Given the system and measurement equations

$$x_k=\Phi_{k,k-1}x_{k-1}+\Gamma_{k-1}u_{k-1}+\Lambda_{k-1}w_{k-1} \tag{9}$$

$$z_k=H_kx_k+v_k \tag{10}$$

where

$x_k\in R^{n\times1}$	State vector
$u_{k-1}\in R^{l_u\times1}$	Input vector
$w_{k-1}\in R^{l_w\times1}$	Plant error vector
$z_k\in R^{m\times1}$	Measurement vector
$v_k\in R^{m\times1}$	Measurement error vector
$\Phi_{k,k-1}\in R^{n\times n}$	State transition matrix
$\Gamma_{k-1}\in R^{n\times l_u}$	Input matrix
$\Lambda_{k-1}\in R^{n\times l_w}$	Plant noise matrix
$\mathrm{H}_k\in R^{m\times n}$	Measurement matrix

the Kalman Filter provides the optimal state estimation through [22]

$$\hat{x}_k^{-}=\Phi_{k,k-1}\hat{x}_{k-1}^{+}+\Gamma_{k-1}u_{k-1} \tag{11}$$

$$P_k^{-}=\Phi_{k,k-1}P_{k-1}^{+}\Phi_{k,k-1}^{T}+\Lambda_{k-1}Q_{k-1}\Lambda_{k-1}^{T} \tag{12}$$

$$K_k=P_k^{-}H_k^{T}\left[H_kP_k^{-}H_k^{T}+R_k\right]^{-1} \tag{13}$$

$$\hat{x}_k^{+}=\hat{x}_k^{-}+K_k\left[z_k-H_k\hat{x}_k^{-}\right] \tag{14}$$

$$P_k^{+}=\left[I-K_kH_k\right]P_k^{-} \tag{15}$$

where

$\hat{x}_k^-(\hat{x}_k^+)$	The predicted (corrected) state estimate
$P_k^-(P_k^+)$	The predicted (corrected) state error covariance
$Q_k \equiv \varepsilon(w_k w_k^T)$	Plant noise covariance matrix
$R_k \equiv \varepsilon(v_k v_k^T)$	Measurement noise covariance matrix

The symbol $\varepsilon(\cdot)$ is an expected value of a random variable. Equations (11)-(12) are referred as 'time update', while (14)-(15) are 'measurement update'. As our system has nonlinear measurement equation, (10) would have the form of

$$z_k = g(x_k) + v_k = \begin{bmatrix} g_1(x_{k,1},\cdots,x_{k,n}) \\ \vdots \\ g_m(x_{k,1},\cdots,x_{k,n}) \end{bmatrix} + v_k \tag{16}$$

In this case, the Jacobian of (16) replaces H_k as

$$H_k = \begin{bmatrix} \frac{\partial g_1}{\partial x_{k,1}} & \frac{\partial g_1}{\partial x_{k,2}} & \cdots & \frac{\partial g_1}{\partial x_{k,n}} \\ \frac{\partial g_2}{\partial x_{k,1}} & \frac{\partial g_2}{\partial x_{k,2}} & \cdots & \frac{\partial g_2}{\partial x_{k,n}} \\ \vdots & \vdots & \ddots & \vdots \\ \frac{\partial g_m}{\partial x_{k,1}} & \frac{\partial g_m}{\partial x_{k,2}} & \cdots & \frac{\partial g_m}{\partial x_{k,n}} \end{bmatrix}_{\hat{x}_k^-} \tag{17}$$

Additionally, (14) is changed to

$$\hat{x}_k^+ = \hat{x}_k^- + K_k\left[z_k - g(\hat{x}_k^-)\right] \tag{18}$$

This whole process is known as the Extended Kalman Filter (EKF). Unlike its linear counterpart, the EKF is not an optimal estimator. However it provides a working solution with low computational requirement.

A. *Time update of the Kalman Filter*

Governing equations for IMU measurements are baselines of the time update equations. Accelerations and angular rate from an IMU are [18]

$$a_{xm} = \dot{U} - V\dot{\psi} + b_x + w_x \tag{19}$$

$$a_{ym} = \dot{V} + U\dot{\psi} + b_y + w_y \tag{20}$$

$$r_m = \dot{\psi} + b_r + w_r \tag{21}$$

where

a_{xm}	Longitudinal acceleration measurement
a_{ym}	Lateral acceleration measurement
r_m	Yaw rate measurement
b_x, b_y, b_r	Biases in a_{xm}, a_{ym}, and r_m
w_x, w_y, w_r	Gaussian white noise in a_{xm}, a_{ym}, and r_m

These equations are rearranged to form a differential equation of (22) and it is the base of the 'time update' equations.

$$\begin{bmatrix} \dot{U} \\ \dot{V} \\ \dot{\psi} \end{bmatrix} = \begin{bmatrix} 0 & \dot{\psi} & 0 \\ -\dot{\psi} & 0 & 0 \\ 0 & 0 & 0 \end{bmatrix}\begin{bmatrix} U \\ V \\ \psi \end{bmatrix} + \begin{bmatrix} 1 & 0 & 0 \\ 0 & 1 & 0 \\ 0 & 0 & 1 \end{bmatrix}\begin{bmatrix} a_{xm} - b_x \\ a_{ym} - b_y \\ r_m - b_r \end{bmatrix} + \begin{bmatrix} 1 & 0 & 0 \\ 0 & 1 & 0 \\ 0 & 0 & 1 \end{bmatrix}\begin{bmatrix} w_x \\ w_y \\ w_r \end{bmatrix} \tag{22}$$

The bias in yaw rate (b_r) can be estimated accurately during vehicle standstill. Biases in accelerometers (b_x, b_y) are calculated by averaging raw signals when a vehicle is driven straight. The bias estimation may not be perfectly accurate. In that case, the sideslip estimation error would be accumulated by integrating (22), which is a main concern of IMU integration-based methods. However, our method makes GPS velocity measurements correct the sideslip estimation during turning. Therefore the impact of inaccurate bias estimation is attenuated compared to pure integration methods.

To implement the Kalman Filter, Equation (22) is rewritten as (23), where $x(t)$ is a state, $u(t)$ is an input and $w(t)$ is a noise. Integration of (22) from t_{k-1} to t_k yields (24) [22].

$$\dot{x}(t) = F(t)x(t) + Gu(t) + Lw(t) \tag{23}$$

$$x(t_k) = \Phi(t_k, t_{k-1})x(t_{k-1}) + \int_{t_{k-1}}^{t_k} \Phi(t_k, \tau)\left[Gu(\tau) + Lw(\tau)\right]d\tau \tag{24}$$

If $\Delta T(\equiv t_k - t_{k-1})$ is small enough, *F(t)* can be handled as a constant matrix (F_{k-1}) within the time step of $[t_{k-1}, t_k)$. Then $\Phi(t_k, t_{k-1})$ is equal to $e^{F_{k-1}\Delta T}$ and (24) becomes

$$x(t_k) = e^{F_{k-1}\Delta T}x(t_{k-1}) + \int_{t_{k-1}}^{t_k} e^{F_{k-1}(t_k-\tau)}Gu(\tau)d\tau + \int_{t_{k-1}}^{t_k} e^{F_{k-1}(t_k-\tau)}Lw(\tau)d\tau \tag{25}$$

ΔT in this study is 6 ms and the input $u(t)$ is the measurement of an IMU. Since the frequency contents of the input (1-4 Hz) are much slower than the sampling rate (166 Hz), $u(\tau)$ in (25) can be handled as a constant equal to $u(t_{k-1})$. However, the same argument is not valid for the plant noise ($w(t)$). Therefore (25) is converted to (26) where x_k is $x(t_k)$ and u_{k-1} is $u(t_{-1})$.

$$x_k = e^{F_{k-1}\Delta T}x_{k-1} + \left[e^{F_{k-1}\Delta T} - I\right]F_{k-1}^{-1}Gu_{k-1} + \int_{t_{k-1}}^{t_k} e^{F_{k-1}(t_k-\tau)}Lw(\tau)d\tau \tag{26}$$

The state estimation follows

$$\hat{x}_k = e^{F_{k-1}\Delta T}\hat{x}_{k-1} + \left[e^{F_{k-1}\Delta T} - I\right]F_{k-1}^{-1}Gu_{k-1} \tag{27}$$

Accordingly, the expected value of the state covariance (P_k) is calculated by (28).

$$P_k \equiv \varepsilon\left\{\left(x_k-\hat{x}_k\right)\left(x_k-\hat{x}_k\right)^T\right\} = e^{F_{k-1}\Delta T}P_{k-1}\left(e^{F_{k-1}\Delta T}\right)^T + \int_{t_{k-1}}^{t_k}\int_{t_{k-1}}^{t_k} e^{F_{k-1}(t_k-\tau)}L\varepsilon\left\{w(\tau)w^T(\alpha)\right\}L^T\left(e^{F_{k-1}(t_k-\alpha)}\right)^T d\alpha d\tau \quad (28)$$

Given $\varepsilon\{w(t)w^T(\tau)\}=Q_c'\delta(t-\tau)$ where Q_c' is the power spectral density matrix and $\delta(t-\tau)$ is the Dirac delta function, (28) is rewritten as

$$P_k = \Phi_{k,k-1}P_{k-1}\Phi_{k,k-1}{}^T + \int_0^{\Delta T} e^{F_{k-1}\tau}LQ_c'L^T\left(e^{F_{k-1}\tau}\right)^T d\tau \quad (29)$$

where $\Phi_{k,k-1}$ is $e^{F_{k-1}\Delta T}$. If ΔT is short compared to the system time constants, $e^{F\Delta T}\approx I+F\Delta T$. Then (27) and (29) become

$$\hat{x}_k = \Phi_{k-1}\hat{x}_{k-1}+\Gamma u_{k-1} \quad (30)$$

$$P_k = \Phi_{k-1}P_{k-1}\Phi_{k-1}{}^T + \Lambda Q_{k-1}'\Lambda^T \quad (31)$$

where $\Gamma=G\Delta T$, $\Lambda=L\Delta T$ and $Q_{k-1}'=\frac{Q_c'}{\Delta T}$. Equations (30)-(31) are derived from a continuous system and they serve as the 'time update' of the Kalman filter.

B. Addressing unsynchronized updates of two GPS receivers

Equations (1)-(2) are used when the front-end GPS receiver has measurement updates and (3)-(4) are used when the rear-end GPS receiver has updates. As two GPS receivers operate independently, their updates are not synchronized (Fig. 5).

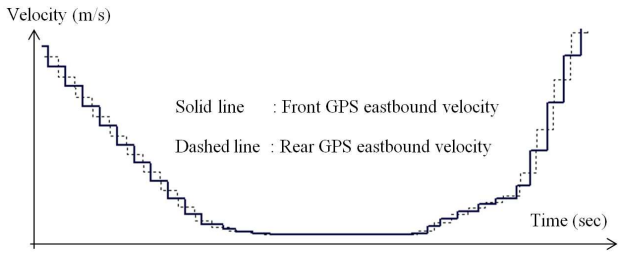

Fig. 5 Typical velocity profiles from two individual GPS receivers.

'Asynchronous update' is an effective technique to solve this problem [23]. The idea is simple: the Kalman filter measurement update is executed only for the updated sensor even though the updated sensor contains only partial information. Therefore, when the front-end GPS receiver is updated, (1)-(2) are used and the measurement matrix would be

$$H_k = \begin{bmatrix} \cos\psi_k & -\sin\psi_k & -U_k\sin\psi_k-(V_k-L_f\dot{\psi}_k)\cos\psi_k \\ \sin\psi_k & \cos\psi_k & U_k\cos\psi_k-(V_k+L_f\dot{\psi}_k)\sin\psi_k \end{bmatrix} \quad (32)$$

When the rear GPS measurement is updated, (3)-(4) are used and the corresponding H_k is

$$H_k = \begin{bmatrix} \cos\psi_k & -\sin\psi_k & -U_k\sin\psi_k-(V_k+L_r\dot{\psi}_k)\cos\psi_k \\ \sin\psi_k & \cos\psi_k & U_k\cos\psi_k-(V_k-L_r\dot{\psi}_k)\sin\psi_k \end{bmatrix} \quad (33)$$

Legitimately, concerns about the observability arise with this method. Results of the observability analysis are presented in Section IV.

C. Addressing significant delays of GPS measurements

GPS velocity measurements have time delays. The GPS receivers used in this research estimate its velocity by interpreting the change in carrier phase between successive samples. This approach is known to have an inherent latency equal to half of the sampling time in delivering velocity measurements [24]. Accordingly, the update frequency of 2.5 Hz would have on average a 200 ms latency solely due to this. Moreover, the internal processing time (<300 ms according to the product specification) of the GPS module and other communication time add to the total delay.

There have been several methods proposed to handle sensor delays and they can be grouped into two categories: hardware-based and software-based methods. In the hardware-based methods, measurement of several sensors can be tightly aligned by using measurement update timing information in a reference clock such as one Pulse-Per-Second signal (PPS) of a GPS [25-27]. However, it requires direct access to the sensor module hardware. As a direct access to the hardware was not allowed in our case, a software-based method was considered. Skog proposed a software-based method using extrapolation through Taylor's expansion [28-29]. We tried this method but the result was often inaccurate under high dynamic maneuvers, such as a double lane change or slalom on high frictional surfaces. Instead, Larsen's 'measurement shifting' idea [30] is adopted. Fig. 6 is a discrete Kalman filter framework to illustrate this idea. From time stamps of s to k-1, the state and its covariance evolve through the time update because no new measurement is available (solid line on the bottom). At the time stamp of k, a measurement is available (z_k) but it represents a value of time s. Accordingly z_k is shifted back to the time s ($z_{k@s}$) and merged with the state estimation of $\hat{x}_s$ to yield the measurement updated state of $\hat{x}_s^{new}$. Then the new state at k ($\hat{x}_k^{new}$) is obtained through time update from $\hat{x}_s^{new}$ (dashed line).

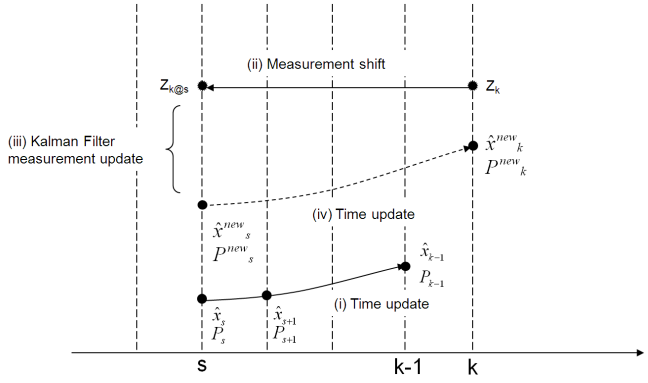

Fig. 6 The measurement shift for delay handling: (i) state estimation through the time update from time index s to k-1, (ii) a measurement is available at k but it is shifted to the time s due to the delay, (iii) the Kalman Filter measurement update at time s, (iv) time update to yield the state estimation at k.

The GPS delay must be known to apply the "measurement shifting" technique. When a vehicle accelerates (or decelerates) during straight driving, the delay in GPS velocity measurements can be observed by comparing it to the vehicle velocity calculated from the wheel speed sensors. Hence the GPS delay is calculated during that maneuver. The vehicle acceleration (or deceleration) must be mild enough to avoid excessive longitudinal wheel slip.

IV. STOCHASTIC OBSERVABILITY ANALYSIS

Even though the Kalman Filter is capable of extracting optimal state estimations from noisy measurements, optimality does not imply stability of the estimation [31]. For linear time invariant (LTI) systems, the necessary and sufficient condition for the estimation stability was identified in a clear form [22]. For time varying systems, however, only sufficient conditions have been developed. A sufficient condition developed by Dyest, Price and Sorenson [32-33] is summarized in Jazwinski's book [31].

The system of (9)-(10) is said to be *uniformly completely observable* if there exists a positive integer N_o and positive constants α_o, β_o such that

$$0 < \alpha_o I \le O(k, k-N_o) \le \beta_o I \quad \forall k \ge N_o$$
$$\text{where}$$
$$O(k, k-N_o) \equiv \sum_{i=k-N_o}^{k} \Phi_{i,k}^T H_i^T R_i^{-1} H_i \Phi_{i,k} \tag{34}$$

The system is *uniformly completely controllable* if there exists a positive integer N_c and positive constants α_c, β_c such that

$$0 < \alpha_c I \le C(k, k-N_c) \le \beta_c I \quad \forall k \ge N_c$$
$$\text{where}$$
$$C(k, k-N_c) \equiv \sum_{i=k-N_c}^{k-1} \Phi_{k,i+1} \Gamma_i Q_i \Gamma_i^T \Phi_{k,i+1}^T \tag{35}$$

For two symmetric matrices A and B, $A \ge B$ means that $(A-B)$ is positive semi-definite. If the system is uniformly completely observable, uniformly completely controllable and P_0 is positive definite, then P_k^+ is uniformly bounded from above and below as

$$0 < \left[O(k,k-N) + C^{-1}(k,k-N)\right]^{-1} \le P_k^+ \le O^{-1}(k,k-N) + C(k,k-N)$$
$$\forall k \ge N \equiv \max(N_o, N_c) \tag{36}$$

Given (36), the state estimation error is *bounded-input bounded-output* (BIBO) stable and the system described by (9) -(10) is said to be *stochastically observable* in the sense that state error covariance matrix (P_k^+) is upper bounded.

The stochastic observability of the Kalman filter is analyzed by investigating three conditions for (36). Since the measurement equation is nonlinear, the Extended Kalman Filter is used for the analysis [34]. Since this is a time-varying system, the observability relies on trajectories of the state. Therefore we established the procedures as follow (i) choose a maneuver, (ii) choose an integer N, (iii) build $O(k, k-N)$ and $C(k, k-N)$ and (iv) evaluate $\{\alpha_o, \beta_o, \alpha_c, \beta_c\}$. If all of $\{\alpha_o, \beta_o, \alpha_c, \beta_c\}$ are positive for a certain choice of N, the system is stochastically observable. Certainly P_0 is initialized to be positive definite.

Test maneuvers include single lane changes (SLC), double lane changes (DLC), slaloms (SLL), and J-turns on high friction surface and N of 1,2 and 3 are tried. The stochastic observability is governed by system matrices (i.e. $\Phi_{k,k-1}, \Gamma_{k-1}$ and H_k of (9)-(10)). In other words, it scrutinizes if the system matrices are properly structured to be observable or not. The unsynchronized GPS measurement updates change the system matrices compared to the synchronized update case. If both GPS receivers update at the same time, H_k would be 4×3 by combining (32) and (33). If not, H_k would be either (32) or (33) according to the updated GPS. Both synchronized/unsynchronized GPS update cases are analyzed to assess the impact of the 'Asynchronous update' technique.

Fig. 7 shows the α_o of $(k, k-N)$, and its corresponding yaw rate during a J-turn maneuver (N=2 case). The solid line represents the synchronized GPS update case and the dash line is for the unsynchronized case. All others of $\{\beta_o, \alpha_c, \beta_c\}$ are positive regardless of vehicle yaw rate, hence α_o is the only limiting factor. In the figure, the dependency of α_o on the yaw rate is clearly visible. When the yaw rate is around zero, α_o is also zero. On the other hand, when the yaw rate is substantial (within the time window 13 sec~18 sec), α_o is positive for the synchronized measurement update case. Consequently, the stochastic observability is guaranteed when the yaw rate is not zero. It should be noted that this result is consistent with the outcome of the singularity analysis in Section II.

The influence of unsynchronized measurement updates is also demonstrated in the figure. As the dashed line is positive during vehicle turning, this Kaman Filter is stochastically

observable even with the unsynchronized measurement update, as long as the vehicle yaw rate is not zero. However, the dashed line is lower than the solid line, implying the observability of the unsynchronized update case is weaker than the synchronized case. Even though a J-turn of N=2 case is presented here, the same conclusion was drawn for different maneuvers and with other N values.

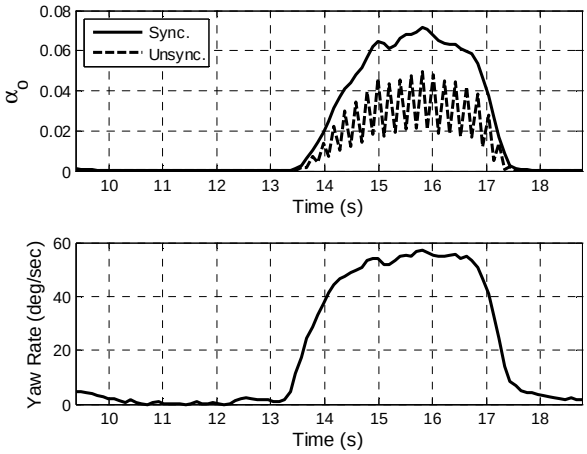

Fig. 7 The minimum eigenvalue (α_o) of $O(k, k-N)$ and its corresponding yaw rate of a J-turn maneuver for N=2

The observability analysis reveals that the proposed method may not estimate the vehicle sideslip accurately during straight driving. The singularity analysis in Section II supports the same conclusion. To resolve this observability concern of straight driving, the bicycle model is utilized. The bicycle model is a kinetic equation which describes vehicle lateral and yaw dynamics as follows

$$\begin{bmatrix} \dot{\beta} \\ \dot{r} \end{bmatrix} = \begin{bmatrix} \frac{-C_f - C_r}{mU} & \frac{-D_f C_f + D_r C_r}{mU^2} - 1 \\ \frac{-D_f C_f + D_r C_r}{I_z} & \frac{-D_f^2 C_f - D_r^2 C_r}{I_z U} \end{bmatrix} \begin{bmatrix} \beta \\ r \end{bmatrix} + \begin{bmatrix} \frac{C_f}{mU} \\ \frac{D_f C_f}{I_z} \end{bmatrix} d \quad (37)$$

where

β	The vehicle sideslip angle
r	Yaw rate
C_f, C_r	Front and rear tire cornering stiffness
D_f, D_r	Distance from CG to front and rear axles
m	Vehicle mass
I_Z	Moment of inertia with respect to z-axis
d	Steering angle at the front axle

Although the bicycle model requires accurate vehicle parameters in general, it can provide fairly accurate vehicle sideslip estimation during straight driving regardless of parameter accuracy. Fig. 8 shows the estimated sideslip by a bicycle model during a lane change on a snow covered road. Vehicle parameters including $C_f, C_f, m,$ and I_z are manipulated to vary from 25% to 175% of nominal values.

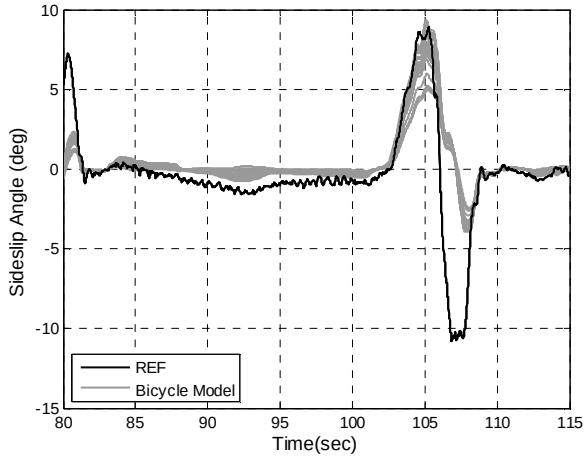

Fig. 8 The vehicle sideslip angle estimations by a bicycle model with parameters of 25%~175% of nominal values at 30 kph.

The black line is the true sideslip angle from the Oxford RT2500 and grey lines represent estimations by the bicycle model with varied parameters. As seen in the figure, sideslip estimation is inaccurate during a lane change maneuver mainly due to the inaccurate tire cornering stiffness. However, it should be noted that sideslip is accurately estimated during straight driving regardless of parameter accuracy. Therefore the bicycle model is solely employed for sideslip estimation during straight driving. The straight driving is determined based on the vehicle yaw rate.

V. EXPERIMENTAL RESULTS

A sports car was used on the TRW proving ground at Locke Township, Michigan to collect the experimental data. Key parameters of the vehicle are shown in Table I. The test vehicle was equipped with a production IMU (from Autoliv) whose update rate is 166 Hz. Sensor noise levels (1σ) are 0.02 m/s^2 for the accelerometer and 0.08^o/sec for the yaw rate gyros. Two units of the U-blox EVK-5H GPS evaluation kit (USD199/each) were utilized. One GPS receiver was installed at the front end of the vehicle, and the other at the rear end. Its noise level (1σ) is 0.01 m/s and its update rate is 2.5 Hz. For the reference signal, an RT2500-250 unit from Oxford Technical Solutions was installed at the vehicle CG. According to its specification document, the error levels (1σ) are 0.3^o for the yaw angle and 0.4^o for the sideslip angle. Its update rate is 250 Hz. Various maneuvers of single lane changes (SLC), double lane changes (DLC), slaloms (SLL), and J-turns were executed on high-/mid-/low-frictional surfaces (asphalt/wet jennite/wet tile, respectively). Each test scenario has 9 repetitions. Therefore, a total of 108 data sets (= 3 surfaces × 4 maneuvers × 9 repetitions) were collected.

TABLE I
TEST VEHICLE PARAMETERS

Wheel base	4.45 m
Front to CG Length (L_f)	1.9 m
CG Height	0.5 m
Vehicle Mass	1765 kg
Yaw Moment of Inertia	2500 kg·m^2

Fig. 9 – Fig. 12 show the sideslip estimation performances with SLC, DLC, SLL, and J-turns. In the top plots, solid lines are the reference values from RT2500 and the dotted lines are estimations from the proposed method. The grey areas show the 95% confidence range calculated from the state error covariance matrices. Since the sideslip estimation accuracy is dependent on the vehicle speed and yaw rate as indicated in (8), bottom plots are added. In the plots, solid lines represent the absolute value of vehicle yaw rates and dotted lines are vehicle velocities. Plots of dry asphalt show higher yaw rates and faster vehicle speeds than plots of wet tile. The J-turn on wet tile shows the yaw rate jump at the end of trace (the bottom right plot of Fig. 12). It is because the vehicle hit the high friction patch at the end of the run and spun out.

To obtain RMS error, the estimation error is tallied only when the magnitude of the vehicle yaw rate is greater than 10 ^{o}/s. The overall RMS error from all the 108 data sets is 2.6^o . Fig. 13 contains boxplots of the sideslip RMS errors, given surface types and maneuvers. The black horizontal line in the grey box represents the median, and the grey box represents the central 50% of the data. Two black horizontal lines outside of the grey box stand for maximum and minimum of the data, respectively. The "+" mark represents an outlier. If this mark appears, a nearby black horizontal line is 1.5 times the height of the central box, instead of a maximum or minimum.

Fig. 13 shows the proposed estimation algorithm performs better on a high friction surface than a low friction surface. On a high friction surface, the RMS error levels are lower and run-to-run variations are tighter. Both features can be explained by (8). First, better accuracy on a high friction surface is a straightforward expectation from (8) because both vehicle speed and yaw rate were higher on the surface. Second, (8) suggests that the standard deviation of the sideslip estimation error has $1/x$ relationship with a vehicle speed and a yaw rate. Accordingly the sideslip estimation error would have higher sensitivity as vehicle speeds and yaw rates are lower. In other words, given the same amount of the yaw rate (or vehicle speed) variations, the standard deviation of the estimation error will vary in wider ranges as the vehicle speed and yaw rate reduce. This is why bottom plots of Fig. 13 have wider ranges.

On the dry asphalt surface, SLL and J-turn show degraded performance than SLC and DLC. This is due to the roll angles generated during maneuvers. Fig. 14 shows the frequency histogram of roll angles generated during maneuvers on the dry asphalt. Black lines represent the combined frequency of SLL and J-turn while grey lines represent that of SLC and DLC. It is clearly observed that more roll angles were generated during SLL /J-turn than SLC/DLC. With 1 ^{o} of roll angles, the gravity exerts 0.17 m/s^2 on a lateral accelerometer and it will work as an unknown bias. Consequently, more roll angles would degrade the estimation accuracy further.

VI. CONCLUSIONS

Horizontal velocities from two GPS receivers were processed to calculate vehicle sideslip angles. Those measurements were integrated with IMU signals including longitudinal/lateral acceleration and yaw rate to compensate for the low update rate of the GPS. The Kalman filter technique was used as the backbone for the sensor fusion. Two challenges are present: (i) delay in GPS signals and (ii) unsynchronized updates between the two GPS receivers. Delays in GPS signals are handled through the 'measurement shift' technique and unsynchronized GPS updates are addressed by 'asynchronous update' technique. The observability analysis reveals that the observability is guaranteed only when the vehicle yaw rate is adequately large. If the vehicle yaw rate is not large enough, the bicycle model is employed for the sideslip angle estimation. To assess the performance, experimental verification included maneuvers of single lane changes, double lane changes, slaloms, and J-turns on three different surface friction levels. The experimental results have shown that the vehicle sideslip angle is estimated fairly accurately regardless of surface friction levels. Accuracy of vehicle parameters such as tire cornering stiffness, mass, and moment of inertia does not influence the estimation performance of the method. The calculated RMS error from 108 data set is 2.6 ^{o}.

Two GPS receivers used in this study cost less than USD 400 (USD 199 each for the full development kit). The IMU price should be in the USD 10 range, considering general market price of ESC systems. Hence the total integration cost is around USD 410 for the single-unit prototype. The price of the GPS receiver was for the enclosed development kit. If just a GPS core chip is used or mass production is involved, costs will drop further. The cost of this method is much lower than that of CDGPS [17-19] because currently a dual-antennae CDGPS costs at least several thousand dollars. This method is similar to single GPS velocity-based method discussed in [13-15]. A fundamental difference is that this method has the sideslip angle estimation corrected by GPS during turning while the single GPS method does not.

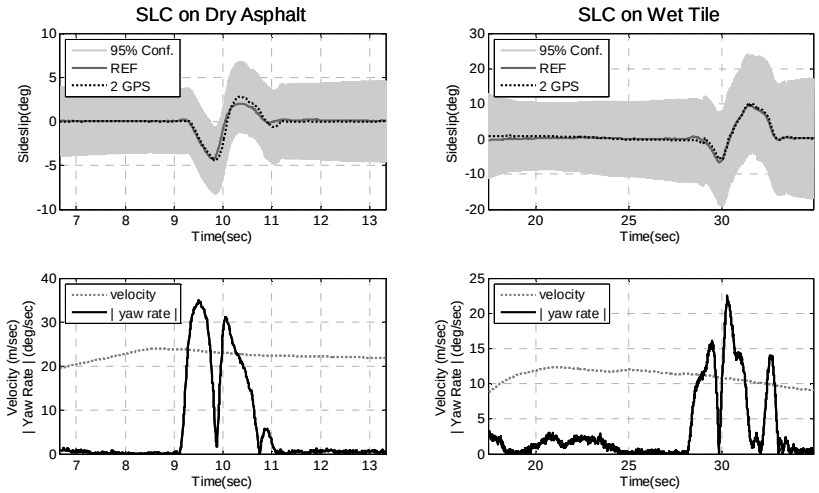

Fig. 9 SLC on dry asphalt and wet tile: the vehicle sideslip estimation and its corresponding velocity and |yaw rate|.

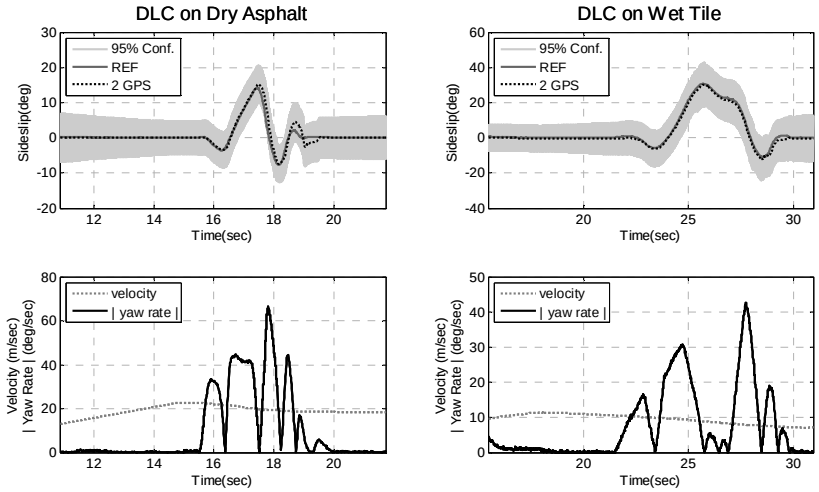

Fig. 10 DLC on dry asphalt and wet tile: the vehicle sideslip estimation and its corresponding velocity and |yaw rate|.

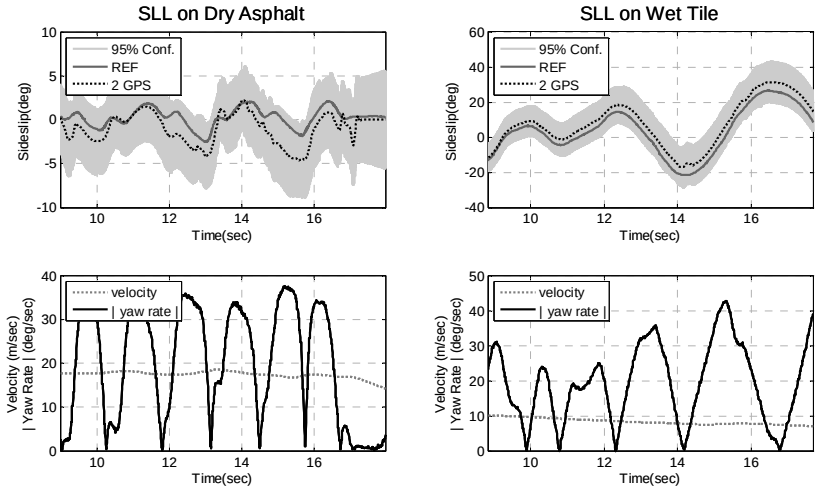

Fig. 11 SLL on dry asphalt and wet tile: the vehicle sideslip estimation and its corresponding velocity and |yaw rate|.

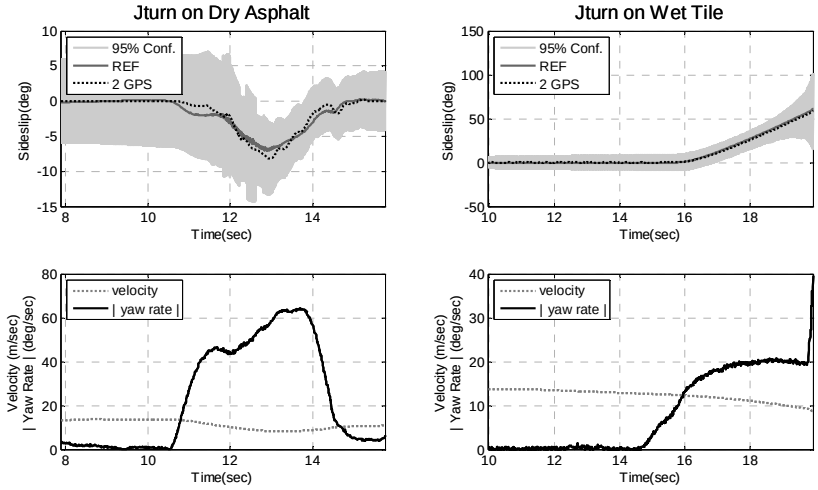

Fig. 12 J-turn on dry asphalt and wet tile: the vehicle sideslip estimation and its corresponding velocity and |yaw rate|.

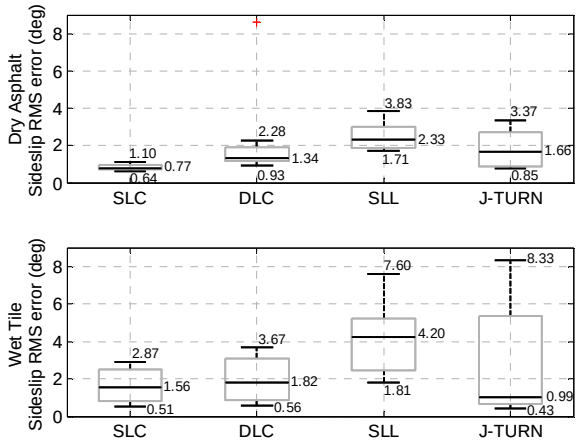

Fig. 13 Distribution of roll angles during a slalom maneuver

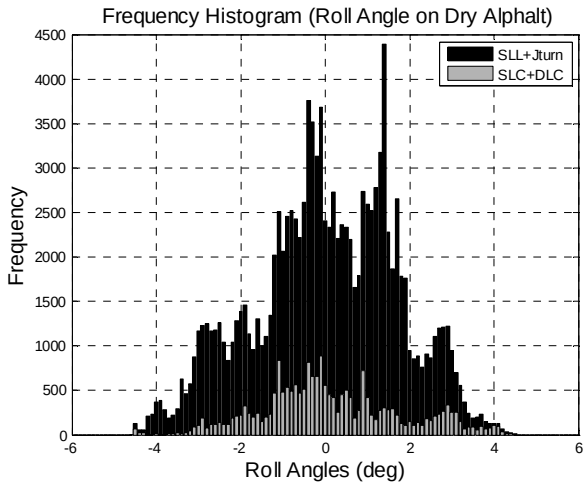

Fig. 14 Frequency histogram of roll angles on a dry asphalt surface

APPENDIX
DERIVATION OF (8)

If the Jacobian matrix of (6) is not singular, solving (6) yields (38) where $L_{sum}=L_f+L_r$. The standard deviation of a linear combination of two variables is computed by

$$\sigma^2(aX+bY)=a^2\sigma^2(X)+b^2\sigma^2(Y)+2abCov(X,Y) \quad (39)$$

Therefore, $\sigma^2(\delta V)$ is calculated by (40). In (40), $cov(\delta V_n, \delta V_e)$ of the front and rear end GPS receivers are assumed to be same. Since $|\sin(\cdot)| \leq 1$, (40) is converted into (41). $\beta = tan^{-1}(V/U) \approx V/U$ if β is small. $\delta\beta \approx \delta V/U$ if U behaves as a constant compared to V. Therefore, (41) is changed to (42) and rearranging (42) yields (8).

$$\delta V = \frac{(-L_r\dot{\psi}\sin\psi + U\cos\psi)\delta V_{fn} + (L_r\dot{\psi}\cos\psi + U\sin\psi)\delta V_{fe} - (L_f\dot{\psi}\sin\psi + U\cos\psi)\delta V_{rn} - (-L_f\dot{\psi}\cos\psi + U\sin\psi)\delta V_{re}}{L_{sum}\dot{\psi}} \tag{38}$$

$$\sigma(\delta V)^2 = \frac{\left(2U^2 + (L_f^2 + L_r^2)\dot{\psi}^2\right)\sigma^2(\delta V_{gps}) + \left[\left(U^2 + L_r^2\dot{\psi}^2\right)\sin(2\psi + \psi_1) + \left(U^2 + L_f^2\dot{\psi}^2\right)\sin(2\psi + \psi_2)\right]Cov(\delta V_n, \delta V_e)}{\left(L_{sum}\dot{\psi}\right)^2} \tag{40}$$

$$where\ \tan\psi_1 = \frac{2L_r\dot{\psi}U}{U^2 - L_r^2\dot{\psi}^2}, \tan\psi_2 = \frac{-2L_f\dot{\psi}U}{U^2 - L_f^2\dot{\psi}^2}, and\ \ Cov(\delta V_{fn}, \delta V_{fe}) = Cov(\delta V_{rn}, \delta V_{re}) \equiv Cov(\delta V_n, \delta V_e)$$

$$\left|\sigma^2(\delta V) - \frac{\left(2U^2 + (L_f^2 + L_r^2)\dot{\psi}^2\right)\sigma^2(\delta V_{gps})}{\left(L_{sum}\dot{\psi}\right)^2}\right| \le \frac{\left(2U^2 + (L_f^2 + L_r^2)\dot{\psi}^2\right)\left|Cov(\delta V_n, \delta V_e)\right|}{\left(L_{sum}\dot{\psi}\right)^2} \tag{41}$$

$$\left|\sigma^2(\delta\beta) - \frac{\left(2U^2 + (L_f^2 + L_r^2)\dot{\psi}^2\right)\sigma^2(\delta V_{gps})}{\left(L_{sum}U\dot{\psi}\right)^2}\right| \le \frac{\left(2U^2 + (L_f^2 + L_r^2)\dot{\psi}^2\right)\left|Cov(\delta V_n, \delta V_e)\right|}{\left(L_{sum}U\dot{\psi}\right)^2} \tag{42}$$

ACKNOWLEDGMENT

The authors would like to thank TRW Automotive for providing the vehicle and facility for testing. Special thanks to Danny Milot of TRW Automotive for his encouragement and support.

REFERENCES

[1] N. H. T. S. Administration, "Federal Motor Vehicle Safety Standards; Electronic Control Systems; Controls and Displays," vol. 72, pp. 17236-17322, 2007.

[2] Y. Shibahata, *et al.*, "Improvement of Vehicle Maneuverability by Direct Yaw Moment Control," *Vehicle System Dynamics*, vol. 22, pp. 465-481, 1993.

[3] J. Farrelly and P. Wellstead, "Esitmation of Vehicle Lateral Velocity," in *IEEE International Conference on Control Applications*, Dearborn, MI, USA, 1996, pp. 552-557.

[4] U. Kiencke and A. Daiss, "Observation of Lateral Vehicle Dynamics," *Control Engineering Practice*, vol. 5, pp. 1145-1150, 1997.

[5] M. C. Best, *et al.*, "An Extended Adaptive Kalman Filter for Real-time State Estimation of Vehicle Handling Dynamics," *Vehicle System Dynamics*, vol. 34, pp. 57-75, 2000.

[6] J. Stephan, *et al.*, "Virtual Sensor: Application to Vehicle Sideslip Angle and Transversal Forces," *IEEE Transactions on Industrial Electronics*, vol. 51, pp. 278-289, 2004.

[7] P. Yih, *et al.*, "Vehicle State Estimation using Steering Torque," in *Proceeding of the 2004 American Control Conference*, Boston, Massachusetts, 2004, pp. 2116-2121.

[8] X. Gao and Z. Yu, "Vehicle Sideslip Angle Estimation by using High Gain Observer," in *AVEC 9th International Symposium on Advanced Vehicle Control*, Kobe, Japan, 2008, pp. 509-514.

[9] H. F. Grip, *et al.*, "Nonlinear Vehicle Side-Slip Estimation with Friction Adaptation," *Automatica*, vol. 44, pp. 611-622, 2008.

[10] T. D. Gillespie, *Fundamentals of Vehicle Dynamics*. Warrendale, PA: Society of Automotive Engineers, Inc., 1992.

[11] L. Imsland, *et al.*, "Vehicle Velocity Estimation using Modular Nonlinear Observers," *Automatica*, vol. 42, pp. 2091-2103, 2006.

[12] A. Y. Ungoren, *et al.*, "Experimental Verification of Lateral Speed Estimation Methods," in *AVEC 6th International Symposium on Advanced Vehicle Control*, Hiroshima,Japan, 2002, pp. 361-366.

[13] D. M. Bevly, "Global Positioning System (GPS): A Low-Cost Velocity Sensor for Correcdting Inertial Sensor Errors on Ground Vehicles," *Journal of Dynamic System, Measurement, and Control*, vol. 126, pp. 255-264, 2004.

[14] D. M. Bevly, *et al.*, "The Use of GPS Based Velocity Measurements for Measurement of Sideslip and Wheel slip," *Vehicle System Dynamics*, vol. 38, pp. 127-147, 2003.

[15] D. M. Bevly, *et al.*, "Integrating INS sensors with GPS Measurements for Continuous Estimation of Vehicle Sideslip, Roll and Tire Cornering Stiffness," *IEEE Transactions on Intelligent Transportation Systems*, vol. 7, pp. 483-493, 2006.

[16] D. Hrovat, *et al.*, "Vehicle Dynamic Measuring Apparatus And Method Using Multiple GPS Antennas," USA Patent, Dec. 30, 2003, 2003.

[17] J. A. Farrell, *et al.*, "Carrier Phase GPS-Aided INS-Based Vehicle Lateral Control," *Journal of Dynamic System, Measurement, and Control*, vol. 125, pp. 339-353, 2003.

[18] J. Ryu and J. C. Gerdes, "Integrating Inertial Sensors with GPS for Vehicle Dynamics Control," *Journal of Dynamic System, Measurement, and Control*, vol. 126, pp. 243-254, 2004.

[19] J. Ryu, *et al.*, "Vehicle Sideslip and Roll Parameter Estimation Using GPS," in *AVEC 6th International Symposium on Advanced Vehicle Control*, Hiroshima,Japan, 2002, pp. 373-380.

[20] D. Piyabongkarn, *et al.*, "Development and Experimental Evaluation of A Slip Angle Estimator for Vehicle Stability Control," in *Proceeding of the 2006 American Control Conference*, Minneapolis, Minnesota, 2006, pp. 5366-5371.

[21] D. Stefanica, *A Primer for the Mathematics of Financial Engineering*. New York: FE Press, 2008.

[22] R. Stengel, *Optimal Control and Estimation*. New York: Dover Publications, Inc., 1994.

[23] R. M. Eustice, *et al.*, "Visually Augmented Navigation for Autonomous Underwater Vehicles," *IEEE Journal of Ocean Engineering*, vol. 33, pp. 103-122, 2008.

[24] J. Ryu, "State and Parameter Estimation For Vehicle Dynamics Control Using GPS," Doctor of Philosophy, Department of Mechanical Engineering, Stanford University, 2004.
[25] D. T. Knight, "Achieving Modularity with Tightly-Coupled GPS/INS," in *Proceeding of the IEEE Plans '92*, Monterey, California, 1992, pp. 426-432.
[26] B. Li, *et al.*, "A GPS-Slaved Time Synchronization System for Hybrid Navigation," *GPS Solutions*, vol. 10, pp. 207-217, 2006.
[27] Q. Li and D. Rus, "Global Clock Synchronization in Sensor Networks," *IEEE Transactions on Computers*, vol. 55, pp. 214-226, 2006.
[28] I. Skog and P. Handel, "A Low-Cost GPS Aided Inertial Navigation System for Vehicle Applications," in *Proceeding of EUSIPCO 2005*, Antalya, Turkey, 2005, pp. 1007-1010.
[29] I. Skog and P. Handel, "Effects of Time Synchronization Errors in GNSS-aided INS," in *Proceedings of Position, Location and Navigation Symposium*, Monterey, California, 2008, pp. 82-88.
[30] T. D. Larsen, *et al.*, "Incorporation of time delayed measurements in a Discrete-time Kalman Filter," in *Proceedings of the 37th IEEE conference on Decision & Control*, Tampa, Florida, 1998, pp. 3972-3977.
[31] A. H. Jazwinski, *Stochastic processes and filtering theory*. New York: Academic Press, 1970.
[32] J. Deyst, John J. and C. F. Price, "Conditions for Asymptotic Stability of the Discrete Minimum-Variance Linear Estimator," IEEE Transactions on Automatic Control, vol. AC-13, pp. 702-705, 1968.
[33] H. W. Sorenson, "On the Error Behavior in Linear Minimum Variance Estimation Problems," IEEE Transactions on Automatic Control, vol. 12, pp. 557-562, 1967.
[34] V. L. Bageshwar, et al., "A Stochastic Observability Test for Discrete-Time Kalman Filters," Journal of Guidance, Control, and Dynamics, vol. 32, pp. 1356-1370, 2009.

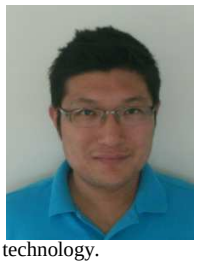

Jong-Hwa Yoon received his B.S. degree from Seoul National University, South Korea, in 2002, and the M.S. and Ph.D. degrees from the University of Michigan, Ann Arbor, in 2004 and 2013, respectively.

He is currently with the vehicle stability control system design department of TRW Automotive, Livonia, MI. His research interests include stochastic filter theory, optimal estimation, vehicle dynamics, vehicle active safety systems, and GPS technology.

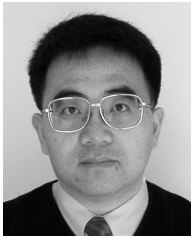

Huei Peng received his Ph.D. from the University of California, Berkeley in 1992. He is currently a Professor at the Department of Mechanical Engineering at the University of Michigan. His research interests include adaptive control and optimal control, with emphasis on their applications to vehicular and transportation systems. His current research focuses include design and control of hybrid vehicles and vehicle active safety systems.

In the last 10 years, he was involved in the design of several military and civilian concept vehicles, including FTTS, FMTV, and Super-HUMMWV—for both electric and hydraulic hybrid vehicle concept designs. He is currently the US Director of the Clean Energy Research Center—Clean Vehicle Consortium, which supports 29 research projects related to the development and analysis of clean vehicles in US and China. He also leads an education project funded by DOE to develop 10 undergraduate and graduate courses including three laboratories courses focusing on transportation electrification. He has more than 200 technical publications, including 85 in referred journals and transactions.

Huei Peng has been an active member of the Society of Automotive Engineers (SAE) and the ASME Dynamic System and Control Division (DSCD). He served as the chair of the ASME DSCD Transportation Panel from 1995 to 1997, and is a member of the Executive Committee of ASME DSCD. He served as an Associate Editor for the IEEE/ASME Transactions on Mechatronics from 1998-2004 and for the ASME Journal of Dynamic Systems, Measurement and Control from 2004-2009. He received the National Science Foundation (NSF) Career award in 1998. He is an ASME Fellow. He is a ChangJiang Scholar at the Tsinghua University.